Journal of Engineering and Natural Sciences
Mühendislik ve Fen Bilimleri Dergisi

Sigma

2004/1

Invited Paper

MODELING OF HETEROSTRUCTURES FOR NANOELECTRONIC DEVICES: TIGHT BINDING VIEW

H. Hakan GÜREL, Özden AKINCI, Hilmi ÜNLÜ*

Department of Physics, Faculty of Science and Letters Computational Science and Engineering Division, Informatics Institute Istanbul Technical University, Maslak-ISTANBUL

Geliş/Received: 12.04.2004

NANOELEKTRONİK İÇİN HETEROYAPILARIN TASARIMI: SIKI BAĞLAM BAKIŞI

ÖZET

Fiziksel ve kimyasal özellikler farklı yarıiletken ince filmlerin büyültülmesinde kaydedilen ilerlemeler elektronik sanayisinde temel bilimsel çalışmaları ve uygulamalarında yeni fırsatlar oluşturdu. Yarıiletken heteroyapıların nano ölçekli elektronik ve optoelektronik cihaz teknolojilerdeki öneminin idrakı, güvenilir ve hassas üretim ve verim tahmininde kullanılan tasarım yöntemlerinin katıhal fiziği ve kuvantum mekaniğinin temel ilkeleri ile uyum içinde olmasına bağlıdır. Bu makalede, nano ölçekli heteroyapı cihazların tasarımında atomik malzeme kuram tabanlı sıkı bağlam kuramı ile tasarımını inceleyeceğiz. Bunlar sp^3 ve sp^3s^* sıkı bağlam kuramları olup kullanılan parametreler yarıiletkenlerin bilinen band yapılarını vermektedir. Bu sıkı bağlam yaklaşımını kullanarak, teknolojide önemli olan AlGaAs/GaAs heteroyapının enerji band yapısının tasarımını inceleyeceğiz. Sıkı bağlam kuramının nano ölçekli aygıtlarda yüklü parçacıkların taşınmasında heteroyapı enerji band yapısının önemini anlamakta faydalı olacağına inanıyoruz.
Anahtar sözcükler: Tasarım, Sıkı bağlam kuramı, Heteroyapılar, Nanoelektronik

ABSTRACT

Advances in growing semiconductor thin films of different physical and chemical properties has provided new opportunities in basic science studies and device applications in electronics industry. Realization of the full potentials of semiconductor heterostructures for nanoscale electronic and optoelectronic device technologies require reliable and precise predictive process and performance simulation models that are consistent with the fundamental principles of solid state physics and quantum mechanics. In this review article, we present a tight binding view of the atomistic materials theory based modeling of heterostructure nanoscale devices. The models are the empirical sp^3 and sp^3s^* tight binding theories in which the parameters are obtained from a fit to the real band structures of semiconductors. Using this scheme, we discuss the modeling of the electronic band structure of technologically important AlGaAs/GaAs heterostructures. We believe that the tight binding theory should be useful in understanding the effects of electronic band structure of heterostructures on charge transport and performance of nanoscale devices.
Keywords: Modeling, Tight Binding Theory, Heterostructures, Nanoelectronics

---

* Sorumlu Yazar/Corresponding Author; e-mail:hunlu@itu.edu.tr, Tel: (212) 285 3201

1. INTRODUCTION

Advances in the processing of semiconductor thin films, opened new ways of thinking in the making of artifical structures for electronic and optical devices that work much faster than conventional silicon devices [1-5]. The use of heterostructures in semiconductor device design allows one to locally modify the energy band structure of the constituents to control the motion of charge carriers. One can artificially change the energy of the moving conduction band and valence band charge carriers across the heterointerface, leading to new device concepts. Due to advances in processing technologies, it is now possible to reduce the device dimensions up to atomic dimensions and to employ one dimensional (1D) nanostructures (superlattices and quantum dots) in electronic and optoelectronic devices [6,7]. The electron confinement in two, one or zero two dimensions in nanostructures are of great interest and have already contributed to the development of new concepts in solid state physics. When the semiconductor composition changes abruptly at interface between constituents, the difference in their energy bands is accommodated by the discontinuities in the conduction and valence bands, shown in Figure 1. Consequently, the energy of the charge carriers at the conduction and valence band edges change across the heterointerface, adding extra driving force to their motion throughout the device.

The impact of heterostructures on the semiconductor physics and device technology is two fold. First, a high charge carrier injection efficiency can be obtained in an anisotype heterojuction in

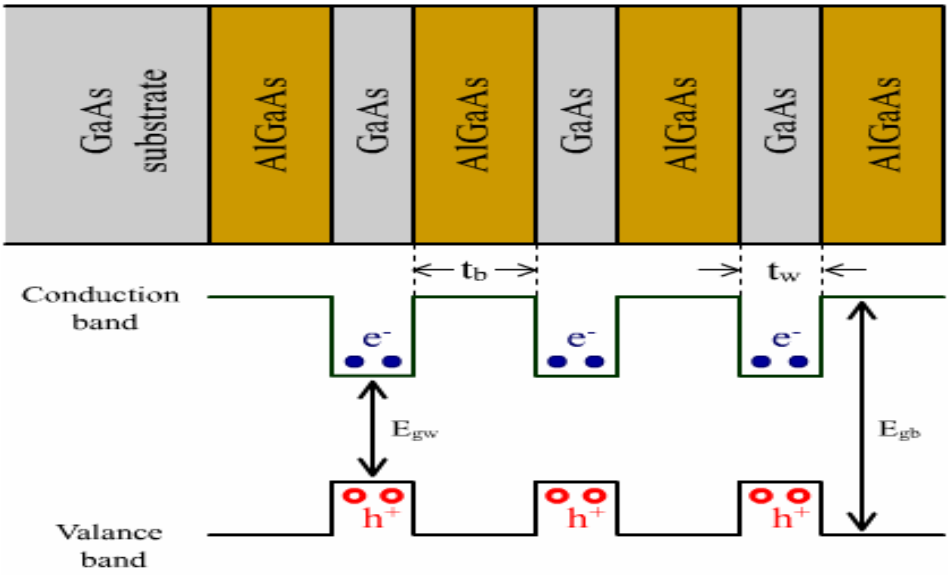

Figure 1. Schematic view of band diagram of abrupt AlGaAs/GaAs multiquantum well

which the charge carriers are flowing from a widegap emitter to narrowgap base, shown in Figure 2. In the operation of heterostructure bipolar transistors (HBTs), the spike ΔE_c in the conduction band and step ΔE_v in the valence band at heteroemitter interface influences the carrier injection and current transport and in turn influence the device performance.

The charge carrier injection factor is particularly related to the conduction and valence band offsets but is often further enhanced by the electric field induced by the charge transfer. Since the potential barrier at heterointerface exists regardless of the base doping level, the base region can be doped heavily to reduce its resistance and the emitter doping can be reduced to minimize its capacitance. Consequently, the use of heteroemitter greatly enhances the emitter current gain and improves the high frequency performance at the same time by reducing the base resistance and base-emitter capacitance [1]. Furthermore, grading of the conduction band across the heteroemitter offers further increase of the base transit velocity.

Second impact of heterostructures on the semiconductor physics and device technology is to confine charge carriers in a narrow bandgap material to reduce their scattering by parent impurities in doped widegap barrier layer of two dimensional structures. The charge carrier scattering that limits the high speed character of metal oxide field effect transistors (MOSFETs) can be minimized by using the heterojunction to separate the free charge carriers in narrowgap quantum well from their parent impurities in doped widegap barrier layer, shown in Figure 3, leading to a much higher mobility and high current from drain to source of a modulation doped field effect transistors (MODFETs) [1]-[5].

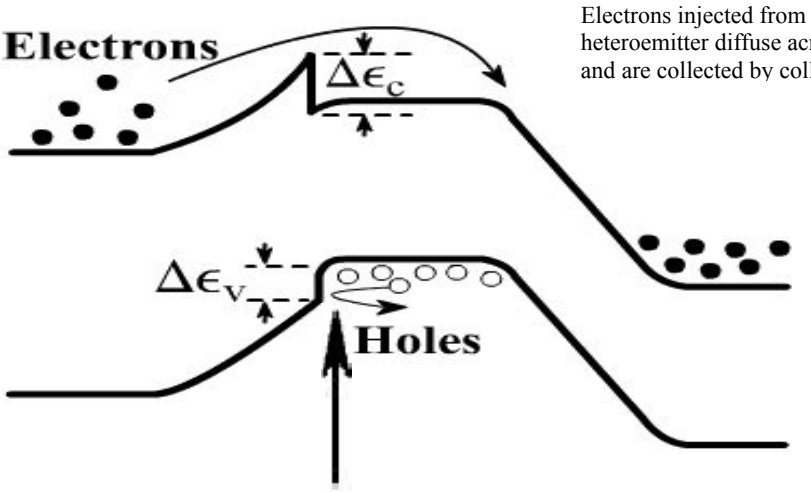

Figure 2. Schematic view of energy band diagram of abrupt heteroemitter Npn AlGaAs/GaAs HBT in forward mode; Emitter junction is forward biased and collector junction is reverse biased

As pointed out above, due to advances in processing technologies, one can now control the alloy composition and doping in ternary and quaternary IV-IV, III-V and II-VI semiconductor compounds over atomic distances, as low as tens of angstroms. Despite the fact that these man-made heterostructures do violate the steady state chemical thermodynamics principles, they are easily grown on GaAs and Si substrates [4],[5] by the highly sophisticated non-equilibrium crystal growth techniques such as MBE and MOCVD. When these advanced growth techniques are combined with the advanced characterization techniques and analysis, impressive number of high performance devices for fast signal processing, and some novel structures that are of interest to solid state scientists and device engineers. The epitaxial layers are so thin that the quantum

mechanical effects, which are important in the operation of heterostructure devices, have been realized. One of the key issues is the understanding the formation and determining the magnitude of conduction and valence band offsets at heterointerfaces, which dominate various device properties such as injection efficiency in HBTs and carrier confinement in MODFETs, and has received considerable attention over the years [8,9].

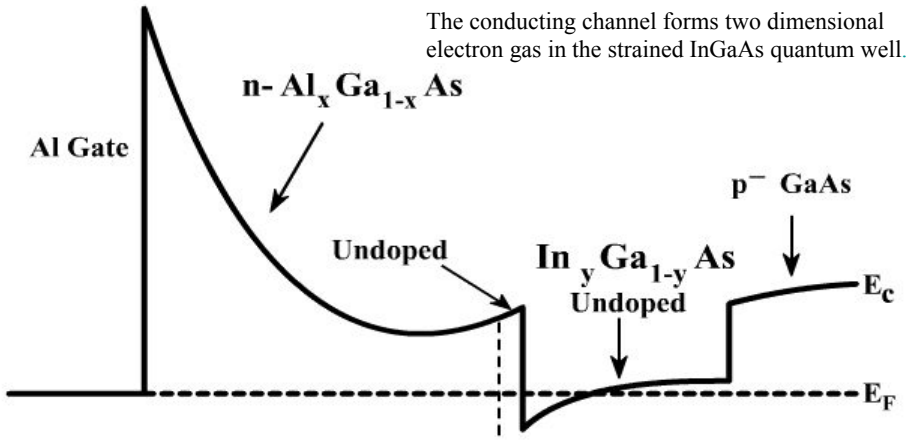

Figure 3. Typical structure for pseudomorpic modulation doped FETs (MODFETs). The narrowgap InGaAs quantum well forms two dimensional electron gas

Advancement in the nanoscale semiconductor device technologies requires reliable and precise predictive process and performance simulation models. Qualitatively reliable and quantitatively precise analytic models are essential in investigating the potential of nanoscale heterostructures for making novel electronic and optical devices. As with all of the semiconductor devices, the key property to understand the impact of heterostructure on the device performance is the electronic energy band structure across the interface. Consequently, theoretical studies of semiconductor nanostructures is highly crucial in the design and optimization of nanoscale devices. In the theoretical studies of nanostructures, the common practice is to use the envelope function approximation (EFA based **k.p** approach which becomes questionable for nanostructure devices such as quantum dots or nanoscale FETs [10]. In this respect, the empirical tight binding modeling is viewed as an attractive way of nanoscale device band structure calculations. In section II, we give a short review of the tight binding modeling of semiconductor structures for nanoscale devices. In section III, the composition and strain effects on bandgaps and band offsets in AlGaAs/GaAs heterostructures are discussed.

2. TIGHT BINDING MODELING OF HETEROSTRUCTURES

In the conventional tight binding theory of semiconductors one assumes that the valence electrons are tightly bound to their nuclei as in the free atom [11,12]. Anion and cation atoms are brought together until their separations becomes comparable to the lattice constant of semiconductors at which their wave functions will overlap. Then the linear combination of basis

functions $\chi_j(k)$ formed by the linear combination of atomic orbitals are used to approximate the electronic wave functions ψ_k of semiconductors, written as

$$\left|\psi_k\right\rangle = \sum_{\alpha} u_\alpha \left|\chi_\alpha(k)\right\rangle = \sum_i \frac{e^{i.k.r_i}}{\sqrt{N_p}} \left|b_\alpha(r-r_i)\right\rangle \tag{1}$$

where **r** is the electron coordinate, **k** is the wave vector, N_p is the number of atoms, and $\mathbf{r}_i$ is the crystal lattice site. The energy state is given by the eigenvalue of the linear equation

$$\sum_{\beta}\left[H_{\alpha\beta}(k) - S_{\alpha\beta}(k)E\right]u_\beta = 0 \tag{2}$$

where E is the energy, $H_{\alpha\beta} = \left\langle \chi_\alpha(k)\right| H \left|\chi_\beta(k)\right\rangle$ is the Hamiltonian matrix and $S_{\alpha\beta} = \left\langle \chi_\alpha(k)\right| \left.\chi_\beta(k)\right\rangle$ is the overlap between the atomic-like orbitals. Here α corresponds to a cation s (p) orbital, β corresponds to an anion s (p) orbital. N_p is the number of the atom pairs, equals to the number of bonds of each type. The position of $\mathbf{r}_i$ is taken to be the midpoint of the corresponding bond. Each eigenstate of the wave number **k** can be written as a linear combination of the eight Bloch sums for that wave number can be written as Eq.(1).

In the case of orthogonal sp3 tight binding formalism [13,14] in which only the nearest neighbor interactions are taken account, the overlap matrix $S_{\alpha\beta}(k)$ is the identity matrix. According to Chadi and Cohen [13,14}, in solving the secular problem given by Eq. (2) one needs to evaluate the following Hamiltonian matrix elements $H_{\alpha\beta} = \left\langle \chi_\alpha(k)\right| H \left|\chi_\beta(k)\right\rangle$

$$\begin{bmatrix}
E_s^c & 0 & 0 & 0 & B_0E_{ss} & B_1E_{sp} & B_2E_{sp} & B_3E_{sp} \\
0 & E_p^c & 0 & 0 & -B_1E_{sp} & B_0E_{xx} & B_3E_{xy} & B_2E_{xy} \\
0 & 0 & E_p^c & 0 & -B_2E_{sp} & B_3E_{xy} & B_0E_{xx} & B_1E_{xy} \\
0 & 0 & 0 & E_p^c & -B_3E_{sp} & B_2E_{xy} & B_1E_{xy} & B_0E_{xx} \\
B_0^*E_{ss} & -B_1^*E_{sp} & B_2^*E_{sp} & B_3^*E_{sp} & E_s^a & 0 & 0 & 0 \\
B_1^*E_{sp} & B_0^*E_{xx} & B_3^*E_{xy} & B_2^*E_{xy} & 0 & E_p^a & 0 & 0 \\
B_2^*E_{sp} & B_3^*E_{xy} & B_0^*E_{xx} & B_1^*E_{xy} & 0 & 0 & E_p^a & 0 \\
B_3^*E_{sp} & B_2^*E_{xy} & B_1^*E_{xy} & B_0^*E_{xx} & 0 & 0 & 0 & E_p^a
\end{bmatrix}$$

where B_i^* is the complex conjugate of B_i matrix element. The diagonal interactions between the same *p* orbitals on each atom yield the symmetric sum, while the off-diagonal interactions yield the asymmetric sums, $\left\langle p_x^c \right| H \left| p_x^a \right\rangle = E_{xx}B_0(k)$, $\left\langle p_x^c \right| H \left| p_y^a \right\rangle = E_{xy}B_3(k)$. In Eq.(2) each $\left\langle s^c \right|$ orbital in the sum making up the state $\left\langle \chi_\alpha(k)\right|$ will have matrix elements $V_{ss\sigma}$ between its four neighboring orbitals $\left|s^a\right\rangle$, each of

these neighboring orbitals enters the matrix element $V_{ss\sigma}$ with a phase factor differing from that of $\left|s^c\right\rangle$ orbital by $e^{ik.d_i}$ with d_i being the vector distance to neighbor. The matrix elements are

$$H_{s^c s^a}(k) = V_{ss\sigma}\sum_i e^{jk.d_i} = V_{ss\sigma}(e^{jk.r_1} + e^{jk.r_2} + e^{jk.r_3} + e^{jk.r_4}) \quad (3)$$

$$\left\langle s^c \left| H \right| s^a \right\rangle = E_{ss}\sum_{i=1}^{4} e^{jk.r_i} = E_{ss}(e^{jk.r_1} + e^{jk.r_2} + e^{jk.r_3} + e^{jk.r_4}) \quad (4)$$

where $j = \sqrt{-1}$ and $r_1 = (a/2)(a_x + a_y + a_z)$, $r_2 = (a/2)(a_x - a_y - a_z)$, $r_3 = (a/2)(-a_x + a_y - a_z)$ and $r_4 = (a/2)(-a_x - a_y + a_z)$ are displacement vectors of the nearest neighbors. Interactions between an *s* orbital of the A atom and p_x, p_y, p_z orbitals of the neighboring B atoms are

$$\left\langle s^c \left| H \right| s^a \right\rangle = E_{ss}(e^{jk.r_1} + e^{jk.r_2} + e^{jk.r_3} + e^{jk.r_4}) = E_{ss}B_0(k)$$
$$\left\langle s^c \left| H \right| p_x^a \right\rangle = E_{sp}(e^{jk.r_1} + e^{jk.r_2} - e^{jk.r_3} - e^{jk.r_4}) = E_{sp}B_1(k)$$
$$\left\langle s^c \left| H \right| p_y^a \right\rangle = E_{sp}(e^{jk.r_1} - e^{jk.r_2} + e^{jk.r_3} - e^{jk.r_4}) = E_{sp}B_2(k)$$
$$\left\langle s^c \left| H \right| p_z^a \right\rangle = E_{sp}(e^{jk.r_1} - e^{jk.r_2} - e^{jk.r_3} - e^{jk.r_4}) = E_{sp}B_3(k)$$

$$B_0(k_x,k_y,k_z) = 4Cos\left(\frac{k_x a}{2}\right)Cos\left(\frac{k_y a}{2}\right)Cos\left(\frac{k_z a}{2}\right) - 4jSin\left(\frac{k_x a}{2}\right)Sin\left(\frac{k_y a}{2}\right)Sin\left(\frac{k_z a}{2}\right)$$

$$B_1(k_x,k_y,k_z) = -4Cos\left(\frac{k_x a}{2}\right)Sin\left(\frac{k_y a}{2}\right)Sin\left(\frac{k_z a}{2}\right) + 4jSin\left(\frac{k_x a}{2}\right)Cos\left(\frac{k_y a}{2}\right)Cos\left(\frac{k_z a}{2}\right)$$

$$B_2(k_x,k_y,k_z) = -4Sin\left(\frac{k_x a}{2}\right)Cos\left(\frac{k_y a}{2}\right)Sin\left(\frac{k_z a}{2}\right) + 4jSin\left(\frac{k_x a}{2}\right)Sin\left(\frac{k_y a}{2}\right)Cos\left(\frac{k_z a}{2}\right)$$

$$B_3(k_x,k_y,k_z) = -4Sin\left(\frac{k_x a}{2}\right)Sin\left(\frac{k_y a}{2}\right)Cos\left(\frac{k_z a}{2}\right) + 4jCos\left(\frac{k_x a}{2}\right)Cos\left(\frac{k_y a}{2}\right)Sin\left(\frac{k_z a}{2}\right)$$

In this matrix, there are nine independent matrix elements, namely the four on-site atomic energies, E_{sa}, E_{sc}, E_{pa} and E_{pc}, with a=anion and c=cation, and five hopping terms, $E_{ss}, E_{xx}, E_{s_a p_c}, E_{s_c p_a}$ and E_{xy}. Provided we have reliable on-site atomic energies, E_{sa}, E_{sc}, E_{pa} and E_{pc}, the realistic TB scheme for determining the off-diagonal matrix elements, $E_{ss}, E_{xx}, E_{s_a p_c}, E_{s_c p_a}$ and E_{xy}, is to focus on producing the nonlocal pesudopotential bands [15] and experimental bandgap data [16]. First two off-diagonal matrix

elements E_{ss} and E_{xx} can be obtained from the bandgap data at Γ symmetry point. For $k=0$ $(k_x=k_y=k_z=0)$, the Block sums B_1, B_2 and B_3 are all zero and B_0 is nonzero. The solution of the energy matrix then yields

$$E(\Gamma_{1c/v})=\frac{1}{2}(E_s^a+E_s^c)\pm\sqrt{[(E_s^a-E_s^c)/2]^2+16E_{ss}^2}$$
$$E(\Gamma_{15c/v})=\frac{1}{2}(E_p^a+E_p^c)\pm\sqrt{[(E_p^a-E_p^c)/2]^2+16E_{xx}^2} \quad (5)$$

The lower Γ_{15} corresponds to the triply degenerate valence band top $\left(E(\Gamma_{15v})\right)$, while the upper Γ_1 corresponds to the bottom of the conduction band $\left(E(\Gamma_{1c})\right)$. The two unknown parameters E_{ss} and E_{xx} can be determined by inverting Eq. (5) provided we have accurate *s* and *p* energies E_s and E_p for the anion and cation atoms, bandgap at Γ and width of the valence band. The next three off-diagonal matrix elements $E_{s_a p_c}, E_{s_c p_a}$ and E_{xy} are obtained from the bandgap data at X and L high symmetry points. At the X symmetry point $(k_x=1, k_y=k_z=0)$ the Block sums $B_0=0, B_1=4i, B_2=0$ and $B_3=0$ and conduction and valence band energies are

$$E(X_{3c/v})=\frac{1}{2}(E_s^a+E_p^c)\pm\sqrt{[(E_s^a-E_p^c)/2]^2+16E_{s_a p_c}^2}$$
$$E(X_{1c/v})=\frac{1}{2}(E_s^a+E_p^c)\pm\sqrt{[(E_s^a-E_p^c)/2]^2+16E_{s_c p_a}^2} \quad (6)$$
$$E(X_{5c/v})=\frac{1}{2}(E_p^a+E_p^c)\pm\sqrt{[(E_p^a-E_p^c)/2]^2+16E_{xy}^2}$$

Finally at L symmetry point $(k_x=k_y=1, k_z=0)$ the conduction and valence band energies are

$$E(L_{3c/v})=\frac{1}{2}(E_p^a+E_p^c)\pm\sqrt{[(E_p^a-E_p^c)/2]^2+4(E_{xx}+E_{xy})^2} \quad (7)$$

Eqs. (6) can be inverted for $E_{s_a p_c}, E_{s_c p_a}$ and E_{xy} interms of the bandgap data at X symmetry point with appropriate s and p energies as defined before. Likewise L energy levels can be improved.

In the empirical sp^3 tight binding modeling of semiconductor band structures, the crucial point is to find the reliable and accurate parameters for the matrix elements that would produce the realistic band structure data such as energy gap, effective mass, etc. Such parametrization is extremely important when dealing with the electronic and optical properties of nanoscale heterostructures. Starting with the original work of Slater and Koster [11] for diamond and InSb, many ETB parametrisations of semiconductors have been made (see Ref. 10 for a detailed review) where the matrix elements were determined by comparing with bandgap data. Simpler form of the ETB parametrization was given by Harrison [12]. In Harrison's approach the diagonal matrix elements are proportional to the atomic ionization energies and the off-diagonal

elements are approximately universal functions of the interatomic spacing. The form, for the simple cubic case, is $V_{ll'm} = \eta_{ll'm} \hbar^2 / md^2$, where m is quantum number, *d* the interatomic distance with $\hbar^2 / m = 7.62 eVA^{o}$. This approach has been used by many to study the physical properties of semiconductors since it yields the overall chemical trends and consistency between different properties with the same universal parameters.

By using the nearest neighbor sp^3 scheme described above, with universal tight binding parameters [12], or with parameters fitted to band structure data [13,14], we can fit in the valence band but not to the conduction bands which is vital in studying the electronic and optical properties of nanoscale heterostructures. In this respect we can use the second nearest neighbor sp3 ETB models [17,18]. Talwar and Ting [17] incorporate the second nearest neighbor interactions of cation and anion atoms in the sp^3 ETB formalism by constructing a nonzero symmetrized (8x8) Hamiltonian matrix with 23 two-center second nearest neighbor integrals. The tight binding Hamiltonian matrix elements $H_{\alpha\beta} = \langle \alpha, k \mid H \mid \beta, k \rangle$ are expressed as

$$H_{\alpha\beta} = E_{\alpha\beta} + \sum_{i \neq 0} I_{\alpha\beta}(0,i) e^{ik.r_i} + H^{"}_{\alpha\beta} \tag{8}$$

where $E_{\alpha\beta}$ represents the intra-atomic integrals ($P_1 - P_4$) which couple atomic orbitals located in the same cell, $I_{\alpha\beta}(0,i)$ represents the nearest neighbor interaction integrals ($P_5 - P_9$) which couples atomic orbitals located in different cells. Last term represents the second nearest neighbor interaction integrals ($P_{10} - P_{23}$). In this approach there are 23 TB parameters to be determined from the fitting of the ETB bands to the nonlocal pseudopotential bands [15] and experimental data at high symmetry points [16]. When compared with nearest neighbor sp^3 ETB model of Chadi and Cohen [13,14], the 2nn sp3 ETB model of Talwar and Ting [17] yields better valence bands, bandgaps and reasonable conduction bands for group III-V compounds.

Choosing a carefully selected set of tight binding parameters one can use the sp3 ETB as the computational scheme to get a good set of energy bands which fit to the experimental data and this has been extensively done over the years. However, it should be pointed out that the emphasis has been on getting the band structure that fits to the observed band extrema and does not pay any attention to getting the charge carrier effective masses at different symmetry points that would agree with the existing experimental data. This becomes important in the modeling and simulation of the charge transport and performance of nanoscale electronic and optoelectronic devices [19-27]. In other words, the nanoscale device performance modeling requires to have accurate numerical values for the electron and hole masses since they determine the charge transport and device performance. In aiming this goal, Loehr and Talwar [18] inverted the Γ, L and X high symmetry point expressions for energy levels, fitting the electron and hole effective masses, to reduce the number of free tight binding parameters from 23 to 8. With the optimized tight binding parameters that reproduce the hight symmetry point energies and effective masses, Loehr and Talwar were successful in investigating the band structure of InAs/InGaSb superlattices. In Table 1, we give list of earlier tight binding parameters of Talwar and Ting [17] and in Table 2 optimized ones for effective masses given by Loehr and Talwar [18]. Using the tight binding parameters of Talwar and his co-workers [17,18], listed in Table 1 and 2 we reproduced the energy band structure of AlAs and GaAs and they are shown in Figure 4. As can be seen from the comparison, the tight binding parameters of Loehr and Talwar [18] yield much

better conduction band energy levels than those of Talwar and Ting [17]. The optimized tight binding parameters of Loehr and Talwar reproduce the electron mass at the lowest conduction valley and heavy hole effective mass of the valence band at Γ point, in addition to its ability to reproduce the correct values of the critical point energies at Γ, L and X symmetry points.

Table 1. 2nn sp^3 ETB model parameters of Talwar and Ting [17] to obtain the energy band structure of bulk AlAs and GaAs

$E(\alpha,\beta)$ at 0K	AlAs	GaAs		AlAs	GaAs
$P_1=E_{ss}(000)0$	-6.1517	-6.7236	$P_{12}=4E_{xy}(1,1,0)0$	0.7600	0.6000
$P_2=E_{ss}(000)1$	-1.9922	-3.9783	$P_{13}=4E_{xy}(1,1,0)1$	1.3300	0.9600
$P_3=E_{xx}(000)0$	1.2107	0.6410	$P_{14}=4E_{xx}(1,1,0)0$	0.5522	0.4445
$P_4=E_{xx}(000)1$	2.3317	2.8741	$P_{15}=4E_{xx}(1,1,0)1$	1.1054	1.1208
$P_5=4E_{ss}(0.5,0.5,0.5)0$	-7.1600	-6.9000	$P_{16}=4E_{sx}(1,1,0)0$	0.0400	0.0452
$P_6=4E_{sx}(0.5,0.5,0.5)01$	5.2520	5.2400	$P_{17}=4E_{sx}(1,1,0)1$	0.0730	0.0964
$P_7=4E_{sx}(0.5,0.5,0.5)10$	4.0500	4.3210	$P_{18}=4E_{ss}(1,1,0)0$	-0.0256	-0.0474
$P_8=4E_{xx}(0.5,0.5,0.5)$	2.0080	2.0000	$P_{19}=4E_{ss}(1,1,0)1$	-0.0765	-0.0653
$P_9=4E_{xy}(0.5,0.5,0.5)$	4.8500	5.5000	$P_{20}=4E_{sx}(0,1,1)0$	0.5400	0.7800
$P_{10}=4E_{xx}(0,1,1)0$	-1.1206	-0.3391	$P_{21}=4E_{sx}(0,1,1)1$	-0.1200	-0.0800
$P_{11}=4E_{xx}(0,1,1)1$	-1.1670	-1.7563	$P_{22}=4E_{xy}(0,1,1)0$	0.00000	0.0000
			$P_{23}=4E_{xy}(0,1,1)1$	0.00000	0.0000

As a major step for developing more refined matrix element parametrization Vogl et al [19] proposed sp^3s^* ETB model by adding the s excited states (termed s*) to the sp^3 basis set*) to account for the high energy orbitals. The general form of sp^3s^* Hamiltonian matrix is [19]:

$$\begin{bmatrix}
E_s^c & 0 & 0 & 0 & 0 & B_0E_{ss} & B_1E_{sp} & B_2E_{sp} & B_3E_{sp} & 0 \\
0 & E_p^c & 0 & 0 & 0 & -B_1E_{ps} & B_0E_{xx} & B_3E_{xy} & B_2E_{xy} & -B_1E_{ps^*} \\
0 & 0 & E_p^c & 0 & 0 & -B_2E_{ps} & B_3E_{xy} & B_0E_{xx} & B_1E_{xy} & -B_2E_{ps^*} \\
0 & 0 & 0 & E_p^c & 0 & -B_3E_{ps} & B_2E_{xy} & B_1E_{xy} & B_0E_{xx} & -B_3E_{ps^*} \\
0 & 0 & 0 & 0 & E_{s^*}^c & 0 & B_1E_{s^*p} & B_2E_{s^*p} & B_3E_{s^*p} & 0 \\
B_0^*E_{ss} & -B_1^*E_{sp} & -B_2^*E_{sp} & -B_3^*E_{sp} & 0 & E_s^a & 0 & 0 & 0 & 0 \\
B_1^*E_{sp} & B_0^*E_{xx} & B_3^*E_{xy} & B_2^*E_{xy} & 0 & 0 & E_p^a & 0 & 0 & 0 \\
B_2^*E_{sp} & B_3^*E_{xy} & B_0^*E_{xx} & B_1^*E_{xy} & 0 & 0 & 0 & E_p^a & 0 & 0 \\
B_3^*E_{sp} & B_2^*E_{xy} & B_1^*E_{xy} & B_0^*E_{xx} & 0 & 0 & 0 & 0 & E_p^a & 0 \\
0 & -B_1^*E_{ps^*} & -B_2^*E_{ps^*} & -B_3^*E_{ps^*} & 0 & 0 & 0 & 0 & 0 & E_{s^*}^a
\end{bmatrix}$$

Table 2. 2nn sp^3 ETB model parameters of Loehr and Talwar [18]to obtain the energy band structure of bulk AlAs and GaAs. (Last two digits were ignored.)

$E(\alpha,\beta)$ at 0K	AlAs	GaAs		AlAs	GaAs
$P_1=E_{ss}(000)0$	-7.649	-9.081	$P_{12}=4E_{xy}(1,1,0)0$	0.739	0.680
$P_2=E_{ss}(000)1$	-1.094	-2.376	$P_{13}=4E_{xy}(1,1,0)1$	-2.498	-2.244
$P_3=E_{xx}(000)0$	-0.699	-1.374	$P_{14}=4E_{xx}(1,1,0)0$	0.396	0.510
$P_4=E_{xx}(000)1$	6.866	7.123	$P_{15}=4E_{xx}(1,1,0)1$	1.071	0.822
$P_5=4E_{ss}(0.5,0.5,0.5)0$	-6.138	-6.146	$P_{16}=4E_{sx}(1,1,0)0$	-1.711	-1.442
$P_6=4E_{sx}(0.5,0.5,0.5)01$	2.289	2.794	$P_{17}=4E_{sx}(1,1,0)1$	0.932	0.509
$P_7=4E_{sx}(0.5,0.5,0.5)10$	4.083	4.624	$P_{18}=4E_{ss}(1,1,0)0$	-0.223	0.048
$P_8=4E_{xx}(0.5,0.5,0.5)$	-0.223	-0.223	$P_{19}=4E_{ss}(1,1,0)1$	0.244	0.094
$P_9=4E_{xy}(0.5,0.5,0.5)$	4.241	4.129	$P_{20}=4E_{sx}(0,1,1)0$	1.279	0.054
$P_{10}=4E_{xx}(0,1,1)0$	-0.087	0.133	$P_{21}=4E_{sx}(0,1,1)1$	-0.822	0.697
$P_{11}=4E_{xx}(0,1,1)1$	-4.451	-4.149	$P_{22}=4E_{xy}(0,1,1)0$	0.000	0.000
			$P_{23}=4E_{xy}(0,1,1)1$	0.000	0.000

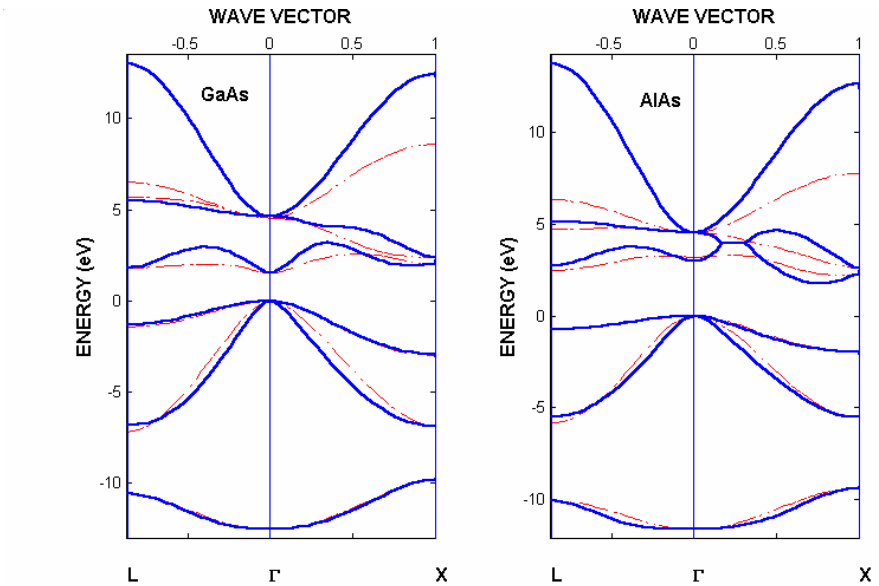

Figure 4. Band structure of GaAs (left) and AlAs (right) using 2nn sp3 ETB model of Talwar and Ting [17] (dashed lines) and 2nn sp3 ETB model of Loeher and Talwar [18] (solid lines)

where B_i^* is the complex conjugate of B_i matrix element. Vogl et al were able to reproduce the conduction and valence band energies of covalently bonded group IV, III-V and II-VI semiconductors with direct and indirect bandgaps. Their conclusion was that the inclusion of the excited s*-state to the sp^3 basis on the cation and anion atoms allows one to better simulate the conduction bands, which cannot be done with the nearest neighbor sp^3 ETB model. Since the proposal of Vogl et al, the nearest neighbor sp^3s^* ETB theory has been used and in so many ways improved by many authors to study the band structure modeling of bulk semiconductors and nanoscale heterostructures [20-27]. In order to see the improvement in the band structure calculations we compare the 2nn sp^3 ETB model of Loehr and Talwar [18] (TB parameters are listed in second colums of Table 1) and the nn sp^3s^* ETB model of Fu and Chao [21] (TB parameters listed in first columns of Table 2) in Figure 5 for GaAs (left) and AlAs (right) at 0 K. band structures calculated by. temperature effects on the semiconductor band structure we used As shown in Figure 5, the improvement by nn sp^3s^* over 2nn sp^3 is clearly visible, especially its ability to predict the temperature effects on the energy levels is apparent at high symmetry points and at varying values of the wave vector over the entire first Brillouin zone.

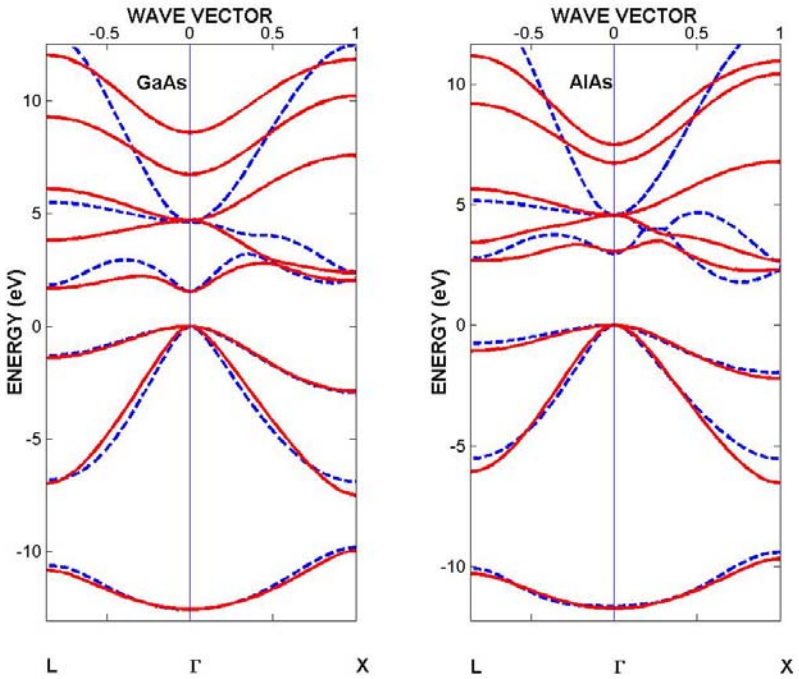

Figure 5. GaAs and AlAs band structures calculated using 2nn sp^3 ETB model of Loehr and Talwar [18] (dashed lines) and nn sp^3s^* ETB model of Fu and Chao [21] (solid lines) at 0K

Perhaps the most remarkable improvement in the sp^3s^* model was made by Boykin and his co-workers [22-25]. They were able to optimize the sp3s* ETB tight binding parameters, with spin-orbit coupling, to reproduce the band structures of III-V compounds, GaAs, AlAs, InAs, GaP, InP, AlP, GaSb, InSb and AlSb, relevant to the simulation of charge carrier transport in nanoscale devices operating at 300 K. In this sp^3s^* ETB view, the better reproduction of charge carrier effective masses at the lowest conduction band and the highest three valence bands is

essential at the expense of the accuracy of other conduction and valence bands since they are considered to be less relevant to the charge transport in nanoscale devices subject to low electric fields at room temperature. In order to see the temperature effects on the semiconductor band structure we used the 0 K and 300 K tight binding parameters, listed in Tabl 2, of Fu and Chao [21] and Klimeck et al [25], respectively, to reproduce the band structure of GaAs and AlAs. As shown in Figure 6, the temperature effects on the energy levels is apparent over the entire Brillouin zone, at high symmetry points and at different values of the wave vector. This conclusion is important in implementing the full band ETB model in the charge transport equations for the reliable performance predictions of nanoscale heterostructure devices (e.g., quantum dots, etc).

Table 3. The nn sp^3s^* ETB model parameters of Fu and Chao [21] at 0K (first columns) and of Klimeck et al [25] at 300 K (second colums) for band structure calculations of GaAs and AlAs

	AlAs		GaAs	
$E(\alpha,\beta)$	Fu and Chao (0K)	Klimeck et al (300 K)	Fu and Chao (0 K)	Klimeck et al (300 K)
E(s,a)	-7.5273	-7.738226	-8.3431	-8.510704
E(p,a)	0.9833	0.872374	1.0414	0.954046
E(s,c)	-1.1627	-1.101736	-2.6569	-2.774754
E(p,c)	3.5867	3.475774	3.6686	3.434046
E(s^*,a)	7.4833	7.373508	6.7386	8.454046
E(s^*,c)	6.7267	6.615774	8.5914	6.584046
V(s,s)	-6.6642	-6.664200	-6.4513	-6.451300
V(x,x)	1.8789	1.878000	1.9546	1.954600
V(x,y)	4.2919	3.860000	5.0779	4.770000
V(sa,p,c)	5.1106	5.600000	4.4800	4.680000
V(sc,pa)	5.4965	6.800000	5.7839	7.700000
V(s^*a,pc)	4.5216	4.220000	4.8422	4.850000
V(pa,s^*c)	4.9950	7.300000	4.8077	7.0100000
Δ_a		0.420000		0.420000
Δ_c		0.024000		0.174000

One of the drawbacks of the sp^3s^* ETB model is its inability to fit the transferse effective mass at the X conduction valley. This limitation can be eliminated by modifying the model to include the second nearest neighbor interactions and/or the number of orbitals. In fact, the nearest neighbor sp^3d5s^* ETB model of Jancu et al [26,27], who added excited d orbitals to the sp^3s^* nearest neighbor approximation with spin-orbit coupling, has been very successful in predicting the band structure of tetrahedrally bonded group IV and III-V compounds. Using the sp^3d5s^* scheme Jancu et al were able to reproduce the X-valley transverse masses in diamond and zincblende semiconductors, including the III-nitrides.

3. RESULTS AND DISCUSSION

The use of heterostructures in semiconductor device design allows one to locally modify the energy band structure of the constituents to control the motion of charge carriers. One can artificially change the energy of the moving conduction band and valence band charge carriers across the heterointerface, leading to new device concepts. Consequently, reliable and precise determination of heterostructure electronic band structure is essential for design and performance predictions of nanoscale electronic and optoelectronic devices. Since most heterostructure devices

use alloy/binary combination (e.g., AlGaAs/GaAs ternary/binary) the first step is to reliably and precisely determine the composition effects on the band structure of alloy semiconductor. Consequently, in the nanoscale device modeling, composition effects on the energy band structure of constituent ternary materials is the central issue. In this respect, the empirical tight binding scheme can be used to incorporate the composition effects for a realistic description of the composition dependent band structure. The common practice is to employ so called the virtual crystal approximation (VCA) to the tight binding Hamiltonian matrix elements and bond length with and without the compositional disorder of the alloy semiconductor. Although the detailed treatement requires the inclusion of compositional disorder effect on the electronic properties [28], we can treat the bond length of alloy semiconductor as nonlinear functions of composition. In the case of ternary $A_xB_{1-x}C$ ternary semiconductor we assume a nonlinear composition dependence of the bond length expressed as

$$d(x) = xd(AC) + (1-x)d(BC) + x(1-x)\Delta d \tag{10}$$

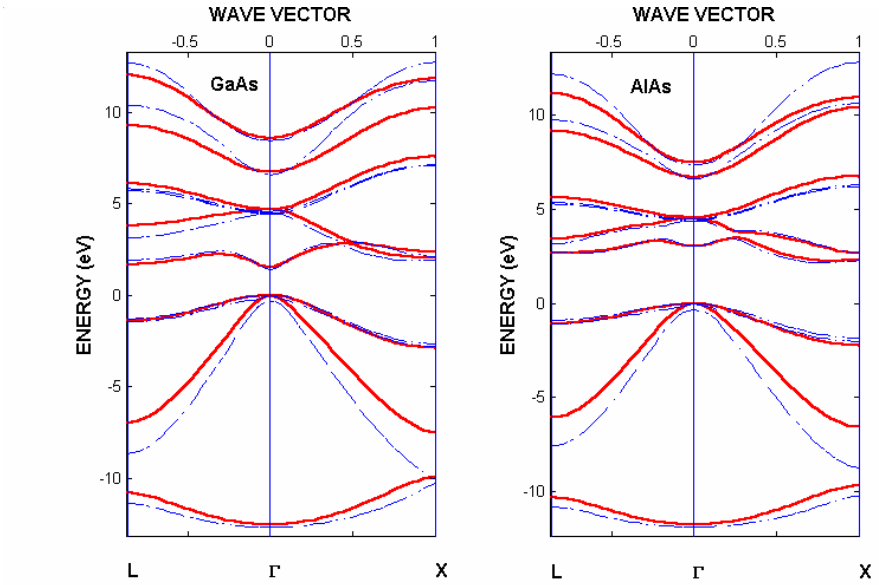

Figure 6. GaAs and AlAs band structures calculated using 0K nn sp^3s^* ETB model of Fu and Chao [21] (dashed line) and the 300 K nn sp^3s^* ETB model of Klimeck et al [25] (solid line)

where $\Delta d = d(AC) - d(BC)$ represents the deviation form the linearity which is a small correction factor in most cases. This allows one to take into account the composition variations of the off-diagonal terms in the tight binding Hamiltonian matrix elements. Likewise, the tight binding parameters representing the diagonal terms in the Hamiltonian matrix for ternary $A_xB_{1-x}C$ ternary semiconductor can be taken linear function of composition as

$$E_{\alpha/\beta}(x) = xE_{\alpha/\beta}(AC) + (1-x)E_{\alpha/\beta}(BC) \tag{11}$$

where $\Delta E_{\alpha/\beta} = E_{\alpha/\beta}(AC) - E_{\alpha/\beta}(BC)$, with α and β representing the fitted energies of the s and p states of the anion and cation atoms forming the AC and BC compounds. This approach has had some success but also some limitations because of the

difficulty in properly describing the composition disorder. Using the tight binding parameters of Loehr and Talwar [18] listed in Table 2 and those of Fu and Chao [21] listed in the first columns of Table 3, we studied the compostion effects on the band structure of AlGaAs ternary semiconductor and the results are displayed in Figures 7 for x=20% and 30% of the Aluminum fraction.

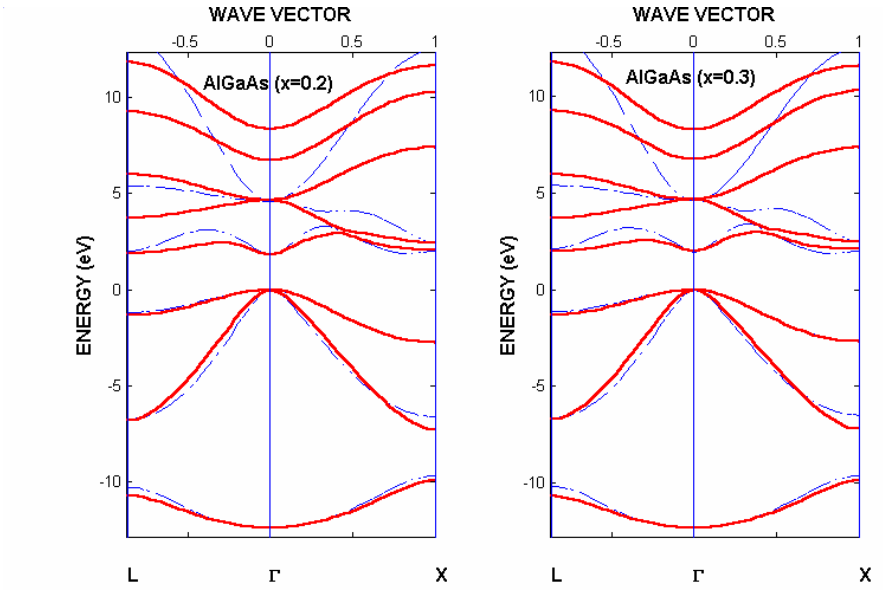

Figure 7. Band structure of AlGaAs with x=0.20 (left) and x=0.30 (right) calculated using the 2nn sp^3 ETB model of Loehr and Talwar [18] (dashed lines) and using the nn sp^3s^* ETB model of Fu and Chao [21] (solid lines) at 0K

As in the case of binary AlAs and GaAs, in order to see the temperature effects on the ternary semiconductor band structure we used the 0 K sp^3s^* ETB model of Fu and Chao and 300 K sp^3s^* ETB model of Klimeck et al [25] with the tight binding parameters of Table 3, allowing composition dependence as described by Eqs. (10) and (11). As shown in Figure 8, the temperature effects on the energy levels at any alloy composition is different at high symmetry points and at different values of the wave vector. Consequently, temperature effects must be seriously considered in implementing the full band ETB models in the charge transport equations for the reliable performance predictions of nanoscale heterostructure devices.

The discussion about the temperature effects on the band structure of ally semiconductors brings us to the discussion of temperature induced strain and lattice mismatch induced interface strain effects on the electronic properties of heterostructures. When two semiconductors with different physical and chemical properties and thicknesses are grown upon each other, the lattice mismatch and thermal expansion gradient over the growth temperature will cause interface strain that will modify the electronic properties of both materials, including the band offsets, and influence the device performance. Limiting the discussion on the technologically important (001) strained heterepitaxy, the shape of the semiconductor crystal unit cell is easily determined by the macroscopic elastic theory. The strain in barrier parallel and perpendicular to the interface are equal to that in the well but are different in the barrier so that we can write

$$\varepsilon_{xx} = \varepsilon_{yy} = \varepsilon_{f//} = \frac{a_{f//} - a_f}{a_f}$$

$$\varepsilon_{zz} = -2\frac{C_{12}}{C_{11}}\varepsilon_{xx} = \varepsilon_{f\perp} = \frac{a_\perp - a_f}{a_f}$$

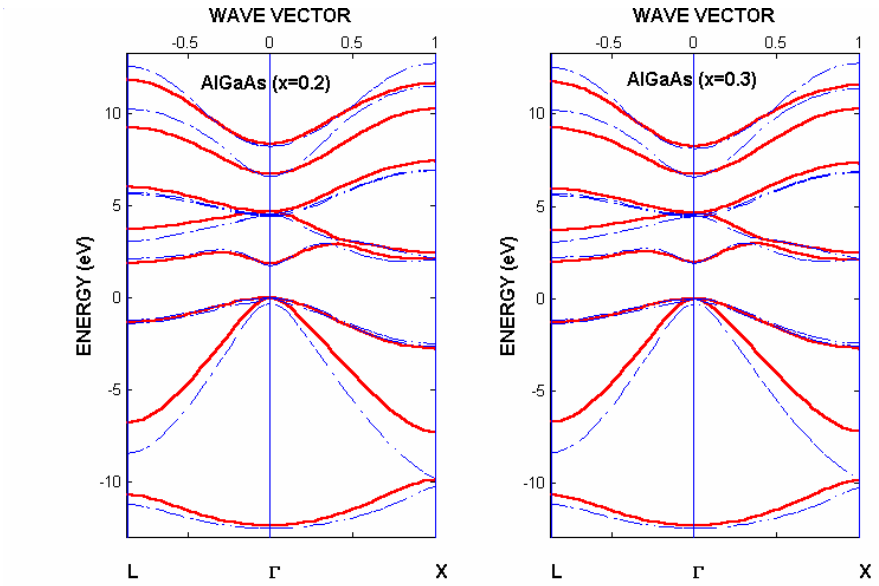

Figure 8. Band structure of AlGaAs with x=0.2 (left) and x=0.3 (right) calculated using nn sp^3s^* model of Fu and Chao [21] (dashed lines) and nn sp^3s^* model of Klimeck et al [25] (solid lines)

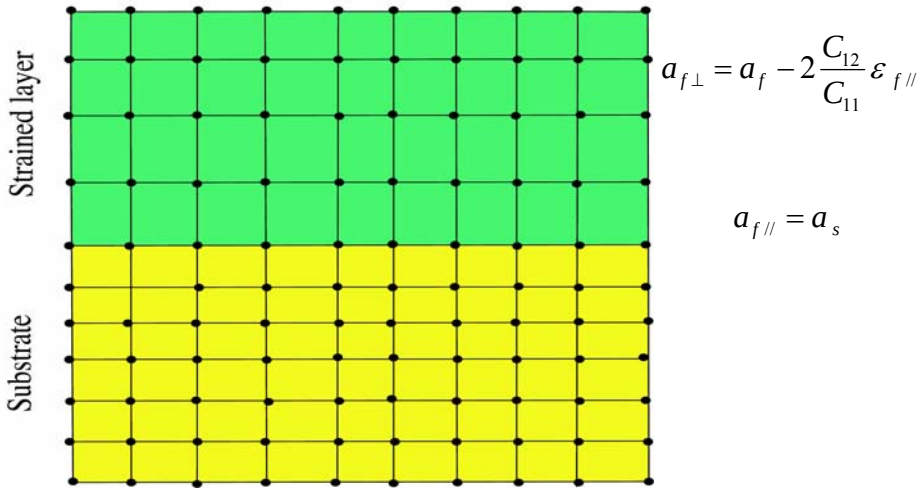

Figure 9. 2D growth of strained thin epilayer on a thick substrate along the [001] direction

The macroscopic observable consequences of lattice mismatch and/or thermal strains are the change in the bandgap energy, effective mass, intrinsic carrier density, and dielectric constant with temperature. The uniaxial component of interface strain splits the heavy-hole, light-hole and split-off valence band edges relative to the average valence band edge and expressed as

$$E_{vh}(\varepsilon) = E_v(\varepsilon) + \frac{1}{3}\Delta - \frac{1}{2}\delta E \tag{12}$$

$$E_{vl}(\varepsilon) = E_v(c) - \frac{1}{6}\Delta + \frac{1}{4}\delta E + \frac{1}{2}\sqrt{\Delta^2 + \Delta\delta E + \frac{9}{4}\delta E^2} \tag{13}$$

$$E_{vs}(\varepsilon) = E_v(c) - \frac{1}{6}\Delta + \frac{1}{4}\delta E - \frac{1}{2}\sqrt{\Delta^2 + \Delta\delta E + \frac{9}{4}\delta E^2} \tag{14}$$

where $\delta E = 2b(\varepsilon_{zz} - \varepsilon_{xx}) = 2b(\varepsilon_{\perp} - \varepsilon_{\parallel})$ and b is the shear deformation potential which describes the splitting in the valence band energy due to the [001] uniaxial strain. $E_v(\varepsilon)$ is the average valence band maximum under hydrostatic component of the biaxial strain. On the other hand, the hydrostatic component shifts the position of the conduction and valence band edges. The shifts in the conduction and valence band energy levels can be written as [9]:

$$E_{cl}(T,P) = E_{cl}(0,P_0) + C_{cP}^0 T(1 - \ln T) - \frac{a_{cl}}{B}[P - \frac{P^2}{2B} - \frac{(1+B')P^3}{6B^2}] \tag{15}$$

$$E_v(T,P) = E_v(0,P_0) + C_{vP}^0 T(1 - \ln T) - \frac{a_v}{B}[P - \frac{P^2}{2B} - \frac{(1+B')P^3}{6B^2}] \tag{16}$$

where P is the pressure. $a_{cl} = -B(\partial E_{cl}/\partial P)$ and $a_v = -B(\partial E_v/\partial P)$ are the conduction and valence band deformation potentials, B is the bulk modulus, $B' = \partial B/\partial P$. The coefficients $C_{cP}^0 = C_{nP}^0 - C_{0P}^0 = C_{pP}^0 + \Delta C_P^0$ and $C_{vP}^0 = C_{pP}^0$ are the standard heat capacities of conduction electrons and valence holes; $C_{nP}^0 = C_{pP}^0 = (5/2)k$, where k is the Boltzmann's constant. $\Delta C_P^0 = C_{nP}^0 + C_{pP}^0 - C_{0P}^0$ is called the heat capacity of reaction for the formation of free conduction electrons and valence holes. ΔC_{lP}^0 is obtained from fitting the bandgap energy $E_{gl}(T,P) = E_{cl}(T,P) - E_v(T,P)$ to the experimental data at constant pressure. Substituting $P = -2B_f C_f \varepsilon_{f\parallel}$ for heterolayer and $P = -3B_s\varepsilon_{s\parallel}$ for substrate for a [001] growth direction one obtains strain dependent conduction and valence band energies. Here $\varepsilon = \varepsilon_{f\parallel} = (a_{f\parallel} - a_f)/a_f$ is the parallel strain in the epilayer, with lattice constant $a_{f\parallel} = a_s$ with a_s being the substrate lattice constant and $C_f = (C_{11} - C_{12})/C_{11}$ is a constant, with elastic constants C_{11} and C_{12} .

The composition effects on the alloy semiconductor band structure at any temperature can also be obtained by combining the Vegard's rule and Kane's three level **k.p** analysis at k=(2π/a)(0; 0; 0) and k=(2π/a)(1; 0; 0) high symmetry points one writes [9]:

$$\frac{1}{m_{n\Gamma}(x)} = \frac{x}{m_{nA\Gamma}(x)} + \frac{1-x}{m_{nB\Gamma}(x)} = 1 + \frac{P_{\Gamma}^2(x)}{3}\left[\frac{2}{E_{g\Gamma}(x)} + \frac{1}{E_{g\Gamma}(x)+\Delta(x)}\right] \quad (17)$$

$$\frac{1}{m_{ntL}(x)} = \frac{x}{m_{ntLA}(x)} + \frac{1-x}{m_{ntLB}(x)} = 1 + P_L^2(x)\left[\frac{2}{E_{gL}(x)} + \frac{1}{E_{gL}(x)+\Delta_L(x)}\right] \quad (18)$$

where $m_{nA\Gamma}(x)$ and $m_{nB\Gamma}(x)$ are the electron effective masses at Γ conduction band valley and m_{ntLA} and m_{ntLB} are the transverse electron effective masses at L conduction valley of binaries AC and BC. $P_{\Gamma}(x) = xP_{A\Gamma} + (1-x)P_{B\Gamma}$ and $P_L(x) = xP_{LA} + (1-x)P_{LB}$ are the momentum matrix elements $\Delta(x) = x\Delta_A + (1-x)\Delta_B$ and $\Delta_L(x) = x\Delta_{LA} + (1-x)\Delta_{LB}$ are the spin-orbit energies. $P_{A\Gamma}, P_{b\Gamma}, P_{AL}$ and P_{BL} of binaries AC and BC are obtained from Eqs. (12) and (13) with measured $m_n(x)$, $m_{ntL}(x)$, $\Delta(x)$ and $\Delta_L(x)$ for x=0 and 1. Inverting Eqs. (12) and (13) one obtains quadratic equations for bandgaps $E_{g\Gamma}(x)$ and $E_{gL}(x)$ and solving the resultant equations yields

$$E_{g\Gamma}(x) = \frac{3/y_{\Gamma}(x) - \Delta(x)}{2} + \frac{1}{2}\left[(\Delta(x) - 3/y_{\Gamma}(x))^2 + 8\Delta(x)/y_{\Gamma}(x)\right]^{1/2} \quad (19)$$

$$E_{gL}(x) = \frac{2/y_L(x) - \Delta_1(x)}{2} + \frac{1}{2}\left[(\Delta_1(x) - 2/y_L(x))^2 + 4\Delta_1(x)/y_L(x)\right]^{1/2} \quad (20)$$

where $y_{\Gamma}(x) = 3(1-m_{n\Gamma}(x))/m_{n\Gamma}(x)P_{\Gamma}^2(x)$ and $y_L(x) = (1-m_{nt\Gamma}(x))/m_{nt\Gamma}(x)P_L^2(x)$. The indirect gap $E_{gX}(x)$ of $A_xB_{1-x}C$ ternary is determined from the following expression

$$E_{gX}(x) = E_{g\Gamma}(x) + [E_{gXA} - E_{g\Gamma A}]x + [E_{gXB} - E_{g\Gamma B}](1-x) \quad (21)$$

$E_{gXA}, E_{gXB,}E_{g\Gamma A},$ and $E_{g\Gamma B}$ are the indirect bandgaps of AC and BC binaries.

As with all of the semiconductor devices, the key property to understand the impact of heterostructure on the device performance is the electronic energy band structure across the interface. When the semiconductor composition changes abruptly at interface between constituents, the difference in their energy bands is accommodated by the discontinuities in the conduction and valence bands, shown in Figure 1. The spike ΔE_c in the conduction band and step in the ΔE_v valence band influences the carrier injection and current transport in heterojunction devices. Since band offsets influence the motion of carriers in the conduction and valence bands (electrons and holes) across the heterointerface, reliable and precise determination of their formation and magnitude is essential for performance predictions of nanoscale heterostructure devices. The magnitude of valence and conduction band offsets at AC/BC heterointerface are determined from the following equations [9]:

$$\Delta E_v = (\frac{E_v}{\varepsilon_\infty})_B - (\frac{E_v}{\varepsilon_\infty})_A, \qquad \Delta E_{ci} = E_{ciA} - E_{ciB} = \Delta E_{gi} - \Delta E_v \tag{22}$$

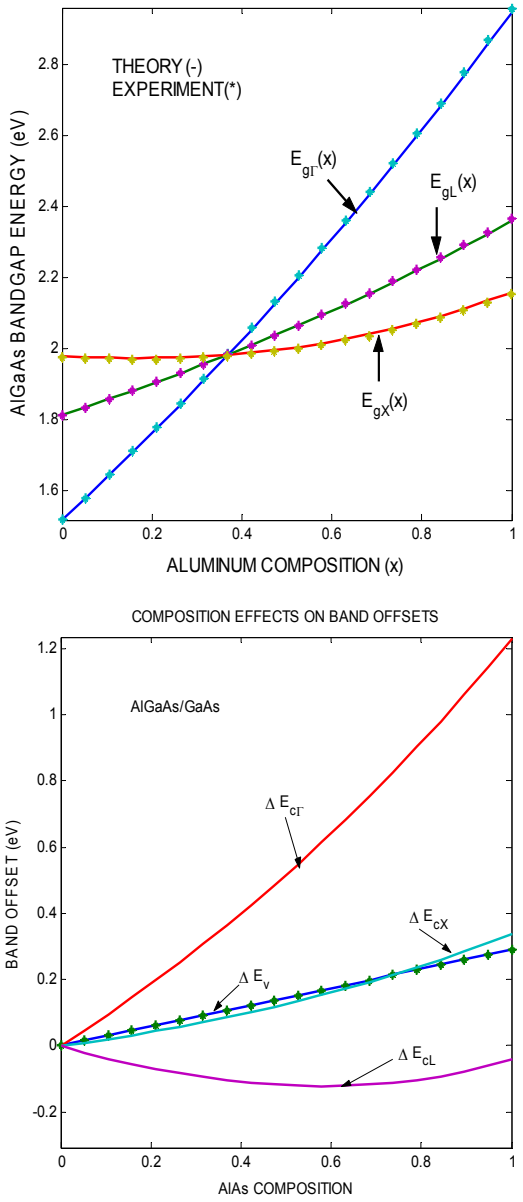

Figure 10. Composition effects on band gaps and band offsets in AlGaAs/GaAs heterostructure

where $E_{ci} = E_{\Gamma_{6c}}, E_{L_{6c}}$ and $E_{X_{6c}}$ conduction bands and $E_{gi} = E_{g\Gamma}, E_{gL}$ and E_{gX} are the lowest bandgaps at k=0($2\pi / a$)(0; 0; 0), k=($2\pi / a$)(1; 0; 0), and k=($2\pi / a$)(1/2; 1/2; 1/2) in the Brillouin zone. $\Delta E_{gi} = E_{gi}(A) - E_{gi}(B)$. $E_{gi}(A)$ and $E_{gi}(B)$ are the bandgaps and $\varepsilon_{\infty}(A)$ and $\varepsilon_{\infty}(B)$ are the optical dielectric constants of AC and BC compounds. Valence band energies are obtained by either using the (a) empirical sp^3 or sp^3s^* tight binding theories described above or (b) using the nonortogonal sp^3 tight binding theory [9]. Figure 10 shows the composition effects on bandgaps and band offsets in AlGaAs/GaAs at room temperature. Results are in good agreement for bandgaps [16] and band offsets [8].

4. SUMMARY

In this paper we have presented the materials theory based modeling technique for the calculation of band structure properties of heterostructures. We showed that the empirical sp^3s^* tight binding model has a considerable potential in the prediction of electronic band structure of heterostructures for nanoelectronic devices. When a widegap ternary semiconductor is grown on a narrowgap binary semiconductor, strain will develop across the interface, caused by the lattice mismatch and thermal expansion gradient over the crystal growth temperature as a function of ternary composition. Any increase in interface strain will modify the heterostructure energy band structure that determines the carrier transport in nanoscale devices. Consequently, reliable and precise determination of the effects of interface strain on the heterostructure electronic band structure is essential for design and performance predictions of nanoscale electronic and optoelectronic devices. The empirical sp^3s^* tight binding model can be used to determine the strain effects on the heterostructure energy bands. The particular advantage of the proposed modeling approach is that it can proceed relatively independently of experiment to provide the potential assessment of new heterostructures at any temperature, strain, alloy composition.

ACKNOWLEDGEMENT

The author acknowledges the financial support by the Research Foundation of Istanbul Technical University: P.NO 965, and by the Scientific and Technical Research Council of Turkey (TÜBITAK): TBAG-1842 (199T061).

REFERENCES

[1] H. Morkoç, H.Ünlü, and G. Ji, Principles and Technology of MODFETs, Vols. 1, 2, Wiley (1991).
[2] H. Ünlü and H. Morkoç, Solid State Technology, 31, 83 (1988).
[3] H. Morkoç and H.Ünlü, in Semiconductors and Semimetals, 24 (R. Dingle, editor), 135 (1987).
[4] H. Ünlü, H. Morkoç, and S. Iyer, in GaAs Technology, 2(D. K. Ferry, ed.) 231 (1990).
[5] H. Morkoç, H.Ünlü, H. Zabel, and N. Otsuka, Solid State Technology, 31, 71 (1988).
[6] J.H. Davies ,The Physics of Low Dimensional Semiconductors (Cambridge: Cambridge Univ. Press) (1998)
[7] Z. I. Alferov and J. A. Lott IEEE J. Sel. Top. In Quantum Electron., 6, 439 (2000).
[8] E. T.Yu, J. O. McCaldin and T. C. McGill, in Solid State Physics, Vol. 46, 1 (1992).
[9] H. Ünlü, Phys. Stat. Sol. (B), 216, 107 (1999); 223, 195 (2001); 229, 581 (2002); 235, 248 (2003, and Comp. Mater. Sci, 21, 453 (2001).
[10] A. Di Carlo, Semicon. Sci. and Technol.,18, R1 (2003).
[11] J. C. Slater and G. F. Koster, Phys. Rev. 94 (1954) 1498

[12] W. A. Harrison, Electronic Structure and the Properties of Solids (San Francisco: Freeman) (1980)
[13] D.J. Chadi and M.L. Cohen, Phys. Status Solidi, 68 405 (1975).
[14] D.J. Chadi, Phys. Rev. B, 16 790 (1977).
[15] M.L. Cohen and J. R. Chelikowsky,Electronic Structure and Optical Properties of Semiconductors (2^{nd} edition), Springer-Verlag (1989).
[16] O. Madelung}(editor), Numerical Data and Functional Relationships in Science and Technology, Part a of Vol. 17, Springer-Verlag (1982) and Part d of Vol. 17, (1984).
[17] D.N. Talwar and C.S. Ting, Phys. Rev. B, 25 2660 (1982).
[18] J.P. Loher and D.N. Talwar, Phys. Rev. B, 55 4353 (1997).
[19] P. Vogl, H. P. Hjalmarson and J. D. Dow, J. Chem. Solids 44 (1983) 365
[20] T.B. Boykin, L.J. Gamble, G. Klimeck and R.C. Bowen, Phys. Rev. B, 59 7301 (1999).
[21] Y. Fu and K. A. Chao, Phys. Rev. B, 43, 4119 (1991).
[22] T.B. Boykin, Phys. Rev. B, 54 8107 (1996).
[23] J.G. Menchero and T.B. Boykin, Phys. Rev. B, 59 8137 (1999).
[24] G. Klimeck R.C. Bowen and T.B. Boykin, Superlattices Microstruct, 29 187 (2001).
[25] G. Klimeck, F. Oyafusoi T. B. Boykin, R. C. Bowen and P. von Allmen l, CMES, 601 (2003)
[26] J.M. Jancu, R. Sholz, F. Beltram and F. Bassani, Phys. Rev. B, 57 6493 (1998).
[27] J.M. Jancu, F. Bassani, F. Della Sala and R. Schols, Appl. Phys. Lett, 81, 4838 (2002).
[28] K. Shim and H. Rabitz, Phys. Rev. B, 57 12874 (1998).